Polymer Testing 113 (2022) 107678

Contents lists available at ScienceDirect

Polymer Testing

journal homepage: www.elsevier.com/locate/polytest

Temperature-dependent fracture behavior of towpreg epoxy resins for cryogenic liquid hydrogen composite vessels: The influence of polysiloxane tougheners on the resin yield behavior

Fabian Hübner [a], Michael Hoffmann [a], Nicole Sommer [a,c], Volker Altstädt [a], Andreas Scherer [b], Tobias Dickhut [b], Holger Ruckdäschel [a,*]

[a] Department of Polymer Engineering, University of Bayreuth, Universitätsstrasse 30, 95447, Bayreuth, Germany
[b] Institute Aeronautical Engineering, Bundeswehr University Munich, Werner-Heisenberg-Weg 39, 85579, Neubiberg, Germany
[c] University of Applied Sciences Hof, Alfons-Goppel-Platz 1, 95028 Hof, Germany

ARTICLE INFO

Keywords:
Fracture toughness
Plastic deformation
Low temperature
Particle-reinforced composites
Fractography

ABSTRACT

In this study, a latent and tacky epoxy resin (EP) modified with siloxane core-shell-particles was developed and investigated. The use of EP as a towpreg matrix for winding of cryogenic composite vessels requires a certain toughness to resist microcracking. First, the mechanical properties at +90 °C, +22 °C, −50 °C and −196 °C were examined, with emphasis on the fracture toughness at cryogenic temperatures. Although the modulus of the resin increased dramatically, the K_{IC} also increased by + 100% at −196 °C. Compression testing revealed that the associated yield point increased up to 500 MPa at −196 °C. The yield point of the modified resins was reduced by almost 10% which leads to easier yielding and enabling toughening mechanisms. Thus, the K_{IC} value clearly is not the primary property that needs to be improved in cryogenics. Second, the radius of the plastic zone around the crack tip (R_p) was calculated. It decreased mathematically from 1.9 μm to 0.4 μm, due to a reduced energy dissipation resulting from a smaller spatial expansion of the plastic deformation zone. Finally, an optimum value of 3% by volume of polydimethylsiloxane was identified, demonstrating an increase of the R_p to 1.8 μm at −196 °C and proving the necessity of combinatorial methods to understand temperature-dependent failure of epoxy matrices.

1. Introduction

Wherever vehicles are in constant motion, lightweight materials are needed to reduce weight to save fuel or enhance load capacities. In recent decades, fiber-reinforced composites made of epoxy resins have attracted great interest in many industrial applications such as aerospace, transportation, sporting goods or automotive [1–3]. Composite hydrogen pressure vessels are subjected to constant tensile loading, for which high-strength materials such as carbon or glass fibers are ideally suited due to their excellent strength-to-density ratio. Therefore, new materials, processing techniques, tests and load optimizations have been of great interest in research and development for several years now [4–9] to further improve the technology and enable a proper entry-to-market [10,11]. Depending on the specific requirements of the products, epoxy resins can be modified regarding T_g, toughness, strength, strain or modulus to achieve a certain behavior with the used fiber [3,12]. When it comes to the storage of low molecular weight hydrogen as an energy carrier, there are two particular options to achieve sufficient volume for energy storage: Gaseous storage under high pressure of at least 700 bar, or liquid storage under 8–12 bar at low temperature below the boiling point at −253 °C [10,13,14]. Therefore, the material properties of a long-term hydrogen-carrying composite vessel have to be studied in detail, especially when dealing with such application environments in a car from −50 to +90 °C or liquid storage in the cryogenic range. Since the structures are rotationally symmetrical to withstand hydrostatic pressure, the parts are manufactured using the wet filament winding process or the improved towpreg or prepreg winding process, which allows faster processing speed and higher quality. Here, the matrix material such as epoxy resin is a material of choice with an excellent price-performance ratio. However, it is known from the literature that in particular the temperature fluctuations that occur during refueling can lead to so-called micro-cracks in the matrix,

* Corresponding author.
E-mail address: ruckdaeschel@uni-bayreuth.de (H. Ruckdäschel).

https://doi.org/10.1016/j.polymertesting.2022.107678
Received 1 March 2022; Received in revised form 19 May 2022; Accepted 18 June 2022
Available online 24 June 2022

which can result in a boil-off [7,12,15,16] or even more fatal explosion accidents. Therefore, efforts have been made ever since, to enhance the toughness of the inherent brittle epoxy matrix. Rubbers [17–20], inorganic silica particles [21–23] among other nano additives such as CNTs [24,25] have been investigated in epoxy resins regarding fracture properties and related micro mechanical phenomena at room temperature for years. In particular, the performance of epoxy resin at low temperatures is of great interest for cryogenic liquid storage vessels. The mechanical behavior was tested in academic resin matrices in quiescent media such as liquid oxygen (−183 °C, 90 K, LOx), liquid nitrogen (−196 °C, 77 K, LN_2) or liquid helium (−269 °C, 4 K, LHe), showing a dependence on the functionality of the epoxy network [26]. Here, it was found that bifunctional epoxy resins tend to stress relax in the cured network, and the fracture toughness was improved by increasing the molecular weight of bifunctional diglycidyl ether of bisphenol A (DGEBA), which means that the crosslink density decreases [27]. In addition to the effect of the resin on the relaxation of the network, there is one major property change in polymers, especially amorphous epoxy resins. Tensile strength increases dramatically, the strain decreases, and modulus increases when the material is exposed to a cold environment. It was found that the tensile strength increases by almost 50% at −196 °C (77 K), regardless of the epoxy resin, crosslinker or therefrom achieved T_g [24,28–31]. In the few publications known which test at −183 °C (90 K), the increase was roughly +50% as well [32,33]. However, there is a positive effect of the tensile strength of construction-related parts. But, the elongation drops massively to a minimum of 2% in the cryogenic state, although the elongation at room temperature was about 4% [33], 10% [30], or 5.5% [24,31]. Additionally, the tensile modulus was found to double almost from room temperature values of 3.0 GPa above 7.5 GPa in several publications [29, 32,33] when obtaining properties in cryogenics. The effects were precisely described by G. Hartwig in 1978 [34] and related to an inter- and intrachain stiffening of the polymer backbone. Hartwig found maximum values of the modulus of epoxy resins between 7300 and 8170 MPa close to the absolute zero at −269 °C (4 K). From this measured embrittlement by stiffened chains, a strong decrease of the fracture toughness would be expected, but many authors including Hartwig stated a contrary strong increase [28,29,32,33,35,36] which was attributed to higher forces required to initiate crack propagation [28]. In summary, from the literature, cryogenic environments lead to a sharp increase in strength and modulus, as well as a decrease in strain independent of the matrix, up to a maximum level of 2%. For the calculation of composite structural parts, the overall yield behavior of the matrix is important. Epoxy resins do not tend to yield under tensile loading either at room temperature or at low temperature. Therefore, compressive loading is of great importance to compare the performance level and brittleness of the matrix as such for the composite. Here, few data were found in the literature to compare Chen et al. at −109 °C, which showed an increase in compressive yield strength from 111 MPa to 303 MPa when the temperature was lowered from +22 °C to −109 °C. A modification with siloxane core-shell particles was carried out to further increase the K_{IC} of the resins. Also, Zhao et al. [29] were aware of the yield behavior of a hyperbranched modification, resulting in an increase from 115 to 390 MPa at −183 °C (90 K). Although overall measured values are available to some extent for certain systems, the micromechanical properties along the fracture mechanics have hardly been described. Therefore, a clear structure-property relationship in cryogenic fracture and flow behavior has not yet been established, which must be truly understood prior to the calculation and design of composite vessels subjected to these conditions. Thus, this study contributes to the understanding of the temperature-dependent behavior from −196 to +90 °C to which towpreg epoxy matrices are subjected in liquid or pressurized hydrogen vessels for automobiles, busses, or the aerospace industry. Modification with toughening polysiloxane particles represents a way to improve plastic deformation, which is drastically reduced in cryogenics.

2. Materials

2.1. Epoxy resins

Two commercial epoxy resins from *Blue Cube Assets GmbH & Co. KG, Olin Epoxy* (Stade, Germany) were used. One bifunctional high viscous base resin (D.E.R. 337™, epoxide equivalent weight EEW = 240 g/mol, repeating unit n = 0.5, see Fig. 1) and a liquid bifunctional carrier resin (D.E.R.331™, EEW = 187 g/mol, repeating unit n = 0.15) were mixed in a ratio of 0.85 to 0.15 for a semi-solid resin consistency at room temperature to derive a tacky behavior for a towpreg or prepreg. This mixture has been investigated concerning tack, curing, one-part storability and processing in our former publication without the incorporation of tougheners [37]. The high M_w D.E.R.337™ was also used due to literature, which expressed enhanced mechanical properties for higher M_w Epoxy.

2.2. Curing agent

Dicyandiamide (DICY) was used as a typical one-part curing agent (DYHARD® 100S of *Alzchem Group AG*, Trostberg, Germany) with a narrow particle size distribution of $d_{98} < 10$ µm [38], which is illustrated in Fig. 2a. To derive a stoichiometric cure state of the epoxy, a theoretical amine equivalent weight of 12.05 g/mol was assumed, which was provided by the supplier. This resulted in a mixing ratio of 100 to 5.25 parts by weight. The accelerator (DYHARD® UR500 from *Alzchem Group AG*, Trostberg, Germany) was also added to lower the typical onset curing temperature of DICY from 160 °C to 125 °C. This catalyst, which acts also as chain extender by NH-functionality, is highlighted in Fig. 2b. Reaction and processing were described precisely in our former publication [37].

The mixing ratio of UR500 comes from literature [39–43] as well as the TDS and is typically 1 pt per 100 pt of resin to achieve accelerated curing avoiding hot-spot formation in samples caused by elevated exothermy in the bulk.

2.3. Polysiloxane toughener

To enhance the mechanical properties of the reference material, a particulate toughening agent, *Genioperl W36* (*Wacker AG, Burghausen, Germany*) was used in 1, 3 and 5% per volume to 100 pt of volume of the whole resin/curing agent/accelerator mixture. The siloxane containing block-copolymeric toughener [44] forms micellic core-shell structures in nanometer sized grape-like domains [45] and shows high toughening efficiency with low concentrations, typical of nano-additives. However, due to the low T_g of the core-shell siloxane of about −140 to −120 °C, this polymer additive is a commercial additive with the lowest available T_g and therefore very interesting for studies in cryogenic environments. Although many other core-shell siloxanes are commercially available [46–48], this particular product was chosen due to its availability without masterbatch or other pre-formulated additive contents that could inadvertently affect its properties.

3. Experimental

3.1. Resin formulation, casting & curing

First, the toughener was added in three different volume concentrations to the semi-solid EP preheated to 80 °C and homogenized for 90 min with a laboratory stirrer in an oil bath at 300 rpm. Then, the liquid EP fraction was mixed with the DICY and UR500 in a planetary mixer (Hauschild Engineering, Hamm, Germany) at 3500 rpm for 2 × 30 s at ambient conditions to disperse the powders uniformly. When the additive flakes were dissolved, the mixture was cooled to 55 °C and the temperature reactive paste was added and stirred at 300 rpm for another 15 min until no agglomerates were visible. The mixture was degassed at

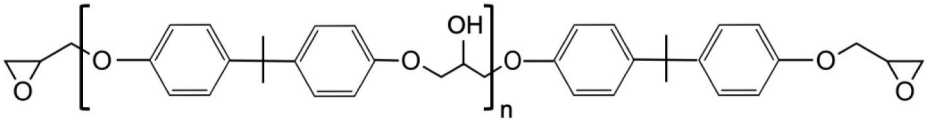

Fig. 1. Molecular structure of bifunctional DGEBA with n = 0.5 for D.E.R. 337™ and n = 0.15 for D.E.R. 331™.

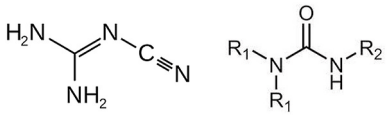

Fig. 2. a) Dicyandiamide DYHARD® 100S and b) Catalyst DYHARD® UR500.

10 mbar for 20 min to avoid subsequent air entrapment in the cured samples. The resins, hardeners, and the toughners form a sticky resin with a viscosity of about 300,000 mPas at 22 °C, but liquid enough for casting at 55 °C [37].

3.2. Sample preparation

The resin was casted in vertical aluminium molds with 200 × 200 × 4 mm^3 and 200 × 200 × 2 mm^3 molds. With a curing cycle of 120 min at 95 °C gelation and pre-curing step and 120 min post-curing at 120 °C, the material was fully cured. Afterwards it was milled into the required geometry according to the testing standards with a precise diamond plate saw (Mutronic Präzisionsgerätebau GmbH & Co. KG, Rieden, Germany).

3.3. Mechanical testing

The materials were tested at four different temperatures, chosen according to several application requirements for pressure vessels. At +90 °C + 22 °C and −50 °C it was tested in air as per the temperature-dependent material property requirements in automotive and transportation. Additionally, −196 °C was chosen, where the samples were immersed throughout the testing to obtain behavior at cryogenic temperatures. The fact that LN_2 is easier and safer to handle with no flammability hazard compared to LH_2, LHe or Lox. This enabled simpler handling and thus broader testing capabilities for the study.

3.3.1. Dynamic-mechanical thermal analysis (DMTA)

The temperature dependent moduli E′, E″ and |E*| of the EP were determined by DMTA measurements between −130 °C and +180 °C. The samples had a geometry of 50 × 10 × 2 mm^3 and were measured in double cantilever mode on a *Netzsch GABO Eplexor 500 N* (Selb, Germany) with a heating rate of 2 K/min at 1 Hz. The deformation chosen was up to 0.1% to measure in the linear elastic regime. The storage modulus E′ and the loss modulus E″ were used for calculating the loss factor tan δ according to equation (1):

$$\tan\ \delta = \frac{E''}{E'} \tag{1}$$

The maximum value of the loss factor was taken to be the primary α-glass transition temperature (T_g) of the cured epoxy resins.

3.3.2. Fracture toughness - Critical stress intensity factor K_{IC} and energy release rate G_{IC}

To quantify the inherent fracture toughness of the resins, the critical stress intensity factor in mode I (K_{IC}) was measured with compact tension specimen (39.6 × 41.25 × 4 mm^3) using a universal testing machine Z020 by Zwick Roell GmbH & Co. KG (Ulm, Germany) equipped with a load cell of 5 kN and a crosshead speed of 10 mm/min. All samples were notched with a 45° angle and a pre-crack was notched with a razorblade. The K_{IC} was calculated according to ISO13586 (equal to the manner of ASTM D5045) and is represented in Eq. (2) [49,50]:

$$K_{IC} = \frac{F_{max}}{d^*\sqrt{w}} \cdot f\left(\frac{a}{w}\right) \tag{2}$$

Here, F_{max} is the force required for crack propagation, d is the sample thickness (4 ± 0.1 mm), w is the measured width of the propagation length and was taken as 33 mm, and f is an extrapolating function depending on the geometry and the actual length of the sharp pre-crack.

The testing at −50, +22 and + 90 °C was carried out in air a thermal chamber equipped with a compressor for cooling and a heater. The cryogenic fracture properties were determined in a bath of liquid nitrogen (−196 °C). Here the samples were fixed and underneath a pneumatic liquid nitrogen bath was elevated around the sample to cover it completely with LN_2. The sample was allowed to reach its equilibrium temperature and after 2 min of cooling, the actual test was performed. Preliminary tests with a temperature sensor showed that the core of the sample quickly reached a temperature of −196 °C due to the cooling capacity of the LN_2 liquid surrounding it. At least five valid samples were considered for evaluation. Subsequently, a median evaluated sample was examined in a scanning electron microscope (SEM) (Zeiss Leo Gemini, Oberkochen, Germany) with an accelerating voltage of 10 kV unsing an Inlens and a backscattering detector were used. Fractographs were taken from a surface pre-sputtered and cleaned with platinum.

The critical energy release rate G in mode I (G_{IC}) based on ISO13586 and was calculated according to equation (3):

$$G_{IC} = \frac{K_{IC}2}{E} \cdot (1 - \nu^2) \tag{3}$$

The K_{IC} was taken from the measurements and ν is the Poisson's ratio, which was assumed to be 0.35 for brittle epoxy. The modulus E refers to the complex magnitude of E′ and E″ expressed by |E*| of the temperature dependent value at −50 °C, +22 °C and +90 °C of DMTA. The |E*| values are represented in Table 1. Since DMTA cannot measure stable tensile moduli in LN_2, the lowest stable value at −130 °C was chosen predictively for the G_{IC} calculation, since this value will not strongly increase as the gamma relaxation of the polymer freezes [51–53]. Hartwig found E-moduli values that vary from 7100 to 7800 MPa for different EP mixtures at −196 °C (77 K), which are 500 MPa higher than those at −130 °C [34]. Thus, E* at −130 °C was used to compare a substituting $G_{IC,}$ to see the effect of the core shell particles on the calculated fracture energy and the change within temperature, even though this value is quantitative and not fully comprehensible.

Table 1
Thermo-mechanical properties derived from DMTA measurements.

	Reference	1 vol% W36	3 vol% W36	5 vol % W36
Loss factor max. T_g/ °C	152	152	148	149
|E*| [MPa] −130 °C	6,850	6,610	6,720	6,530
|E*| [MPa] −50 °C	3,790	3,670	3,510	3,390
|E*| [MPa] +22 °C	2,880	2,810	2,690	2,600
|E*| [MPa] +90 °C	2,080	2,120	2,030	1,950

However, the effect on the T_g drop and peak tan δ is very small even when 5 vol% of the additive is mixed in. The additive provides a good compromise between affecting the network through mobility, which allows toughness, a constant modulus and T_g over a wide temperature range.

3.3.3. Compression properties

Since brittle thermosets do not yield under tension load, especially in low temperature environments, the compression yield properties of the materials were determined according to DIN EN 604 with sample geometries of 10 × 10 × 4 mm^3 with Eq. (4):

$$\sigma_{YC} = \frac{F_Y}{A} \tag{4}$$

Here, the compressive yield strength σ_{YC} is calculated using the force F when the material starts to yield, and the cross-sectional area A is 40 mm^2. The test procedure was performed at −50 °C, +22 °C and +90 °C in the same Zwick Roell Z020 universal testing machine, equipped with a 20 kN load cell. As extremely high forces in excess of 20 kN were recorded in the cryogenic condition, this test was carried out using a Z100 equipped with a 100 kN load cell. The procedure involved placing the specimen in the machine and applying a pre-load of 20 N with the top stamp. Then LN_2 was filled in and due to shrinkage, the preload decreased to 2–5 N. After 2 min of cooling, the actual measurement was performed.

3.3.4. Determination of the plastic zone

The K_{IC} is highly dependent on the required force for crack propagation but it neither accounts for the modulus of the sample nor does it explain detailed crack growth behavior. The radius of the plastic zone reflects the direct toughness of the material and varies from a tenth of a micron in brittle thermosets to several millimeters in tough thermoplastics. The bigger the plastic zone is, the higher the energy that can be dissipated during crack propagation by yielding of the material. This depends strongly on the material itself, testing temperature and deformation rates [54]. Thus, the radius of the plastic zone around a propagating crack tip can be calculated by equation (5) [55–57]:

$$R_p = \frac{1}{6\pi}\left(\frac{K_{IC}}{\sigma_Y}\right)2 \tag{5}$$

Here K_{IC} is the fracture toughness and the pre factor $\frac{1}{6\pi}$ is taken for plane-strain behavior of brittle epoxy. The yield strength σ_Y is usually derived from tensile testing, but Sultan et al. [58] proposed a pre-factor of roughly 0.793 ($\frac{\sqrt{3}-\mu}{\sqrt{3}+\mu}$ with $\mu = 0.2$) to convert compression strength σ_{Yc} to tensile yield stress σ_Y, which was used by other authors as well [55,57,59].

4. Results

4.1. Dynamic mechanical thermal analysis – T_g & storage modulus

First, the thermal behavior of the manufactured epoxy resins was investigated via DMTA measurements over a broad temperature range, which is illustrated in Fig. 3.

Here, the typical behavior of a constantly dropping modulus E' is visible which is typical for an amorphous polymer like epoxy resin [52,60]. From low to high temperature, the materials undergo a softening in different stages. At the lowest measured temperature at −130 °C, the modulus is drastically higher than at room temperature which comes from a stiffening of the aromatic rings of the DGEBA molecule, the so-called β-relaxation until −50 °C. This sub glass transition molecular motion has a great impact on the modulus and stiffness of such materials. A further stiffening would be expected below −130 °C as the γ-transition (local CH_3 sidegroups) would stop flipping and rotating [51,52].

The toughener leads to a reduction in modulus at both, −130 °C and −50 °C. The reason for the lower modulus is the interaction between the stiff epoxy network and the particulate siloxane additive W36. The exact values of all mixtures are represented in Table 1. After β-relaxation, the modulus reaches a plateau around 2.7 GPa, which is the expected value of the thermoset at room temperature. Thermosets are usually used at room temperature or higher temperatures due to their high modulus, which is constant from room temperature to about 100 °C without much softening. This potentially results in an excellent transfer of changing stiffness and strength to the fiber composite. Finally, E′ transitions to the rubbery state, which begins in the range of 120–130 °C. This is the α-relaxation (known as T_g) where the entire molecular network moves. Overall, the modulus decreases linearly with increasing incorporation of the toughening agent. This indicates a softening of the material due to the plasticization of the three-dimensional cross-linked network. Thus, the T_g of DMTA is represented in Fig. 4a.

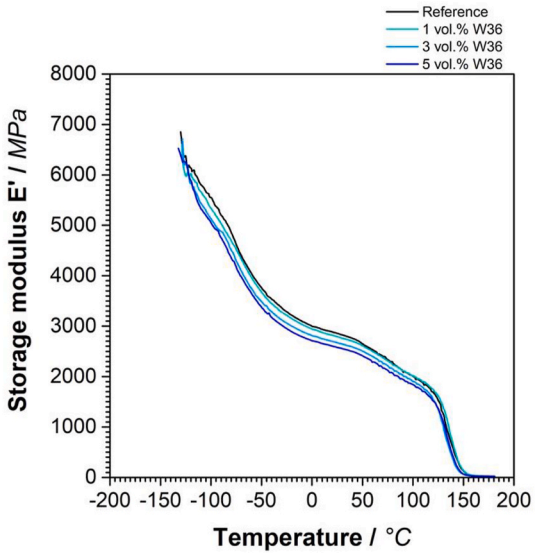

Fig. 3. Dynamic-mechanical thermal analysis - Storage moduli E‘ of reference and toughened epoxy systems from −130 to +180 °C.

The T_g of the systems as well as the shift trend can be extracted from Fig. 4a and Table 1. A slight drop in T_g from 152 °C to a minimum of 148 °C can be seen, although the effect on network quality is very small due to a very sharp tan δ peak. Normally additives, especially rubber tougheners have a strong effect on the crosslink density of the material, leading to a huge drop in modulus and T_g. Genioperl W36 reduces the thermo-mechanical properties of the materials only slightly in this case. Fig. 4b shows aforementioned β-relaxation in detail with a peak at −65 °C. Here, the height of the peak is slightly affected, indicating increased mobility of the systems by the toughener which was already partially presented in literature for plasticizing molecules [61].

4.2. Fracture toughness

In contrast to the constant dynamic-mechanical thermal properties, the influence on the fracture toughness and the resulting fracture energy is drastic, as highlighted in Fig. 5a and b.

The fracture behavior depends strongly on the test temperature, as can be seen from Fig. 5a and the detailed values in Table 2. Surprisingly, all materials show a local minimum at room temperature. Here the reference shows a normal standard of 0.54 MPa $m^{1/2}$, which was gradually increased at 5 vol% W36 to a level of 0.86 MPa $m^{1/2}$. At higher temperatures, the network becomes more mobile, as previously noted in the DMTA measurements, which increases both the toughenability of the network and thus the K_{IC}, i.e. the efficiency of the toughener compared to the reference. At low temperatures, several phenomena are worth highlighting. An increase in the K_{IC} for the reference is shown in black. This is due to the contraction of the network, as already described in the literature [29,30,62,63], leading to a higher force required to break the bonds and propagate the crack in the CT samples, as well as a doubling of the K_{IC} at −196 °C to 1.1 MPa $m^{1/2}$. Moreover, the active participation of siloxane particles in the fracture phenomena is

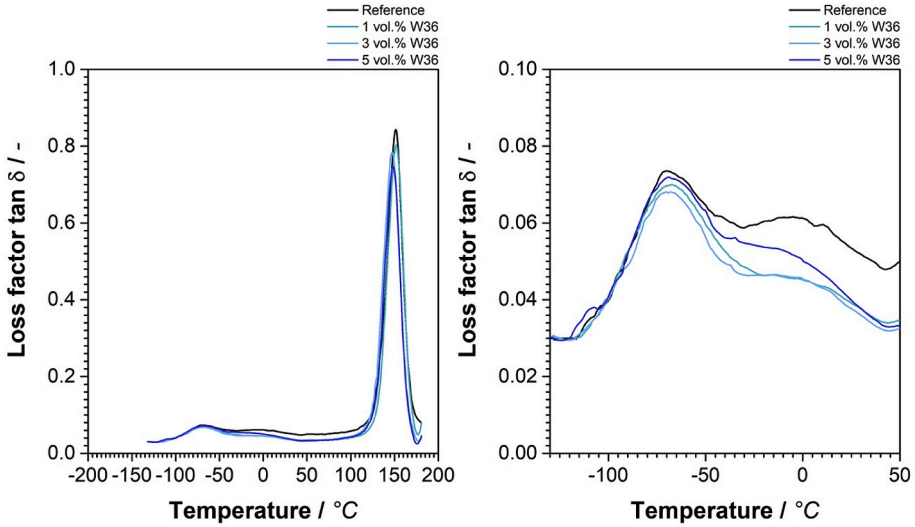

Fig. 4. a) Loss factor tan δ from −130 to +200 °C and b) Highlighted loss factor tan δ in the regime of the β-relaxation.

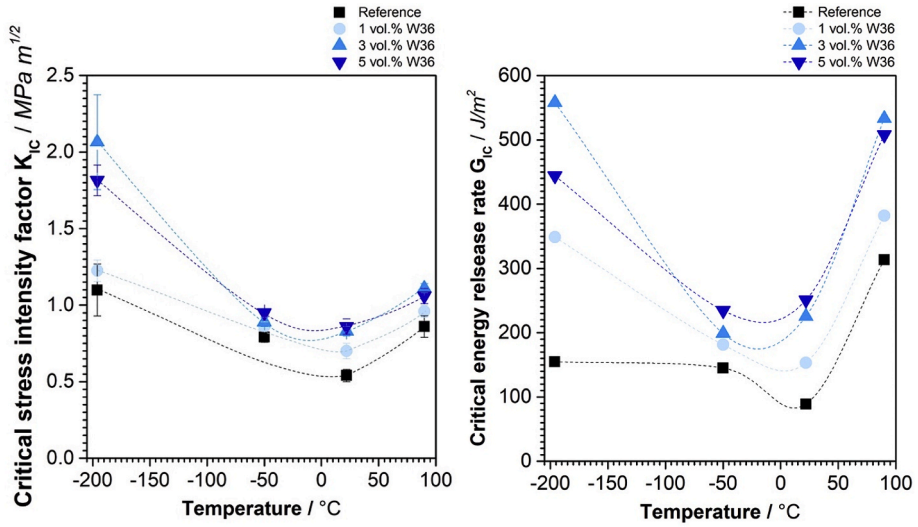

Fig. 5. a: Fracture toughness K_{IC} expressed by the critical stress intensity factor K in mode I and b) critical energy release rate G_{IC} calculated by derived measurements of K_{IC} and |E*| from DMTA at −196 °C, −50 °C, +22 °C and +90 °C.

demonstrated here. At −50 °C, the K_{IC} value increases slightly with increasing particle amount, which is due to the low T_g of the particle core, which is in the rubbery state here. However, at −196 °C, where everything should be "frozen", the value increases even more, reaching 2.07 MPa $m^{1/2}$ at 3% by volume. As described earlier, the K_{IC} correlates directly with the force required for crack propagation at the sharp notch related to Equation (2). But the actual fracture energy, which depends on the stiffness of the specimen or the modulus |E*| of the material, is shown in the graph G_{IC} versus temperature in Fig. 5b and supported by fractographies in chapter 4.4. It can be clearly seen that the trend of a local minimum at room temperature is the same, but the fracture energy G_{IC} as a more quantitative indicator of fracture toughness increases dramatically at +90 °C due to the lower modulus, although K_{IC} is dramatically lower than at −196 °C. A stronger increase of the reference in the range of −50 to −196 can be seen, which is attributed to the strong increase of modulus but moderate increase of K_{IC} resulting in a somewhat constant G_{IC}. Here, the expression of higher toughness is reduced at low temperatures, but with the higher modulus above 6.0 GPa for all samples, the increase in toughness is still present and cannot be associated only with the higher forces required for crack propagation that come from higher atomic bonds at −196 °C.

4.3. Fracture mechanisms - SEM micrographs

All K_{IC} samples tested at the different temperatures were investigated with the SEM. Fig. 6 shows a comparative macroscopic overview, while a detailed assessment is shown in Fig. 7. Both figures clearly reveal why using 3 vol% additive is on the same toughness level as 5 vol% and where the strong push from 1 vol% to 3 vol% in fracture toughness comes from.

A macroscopic yielding effect of the EP itself at the different temperatures of the reference is clearly supported here. While the non-toughened reference shows very pronounced so-called "river lines" at +90 and −196 °C, these fracture bands become smaller and almost disappear at +22 °C. This confirms the qualitative K_{IC} and quantitative G_{IC} measurements. This was somehow expected at higher temperatures, but not at cryogenic temperatures, where extreme embrittlement of polymeric materials is normally expected to cause sudden fracture due to rapidly propagating cracks in bulk materials. Nevertheless, the energy dissipation, i.e. the energy required to open a crack front, is significantly

Table 2
Fracture mechanical properties derived from K_{IC} testing at four different temperatures.

	Reference	1 vol% W36	3 vol% W36	5 vol % W36
K_{IC} [MPa·m$^{1/2}$] −196 °C	1.1 ± 0.17	1.26 ± 0.07	**2.07 ± 0.31**	1.82 ± 0.1
K_{IC} [MPa·m$^{1/2}$] −50 °C	0.79 ± 0.03	0.87 ± 0.02	0.89 ± 0.03	0.95 ± 0.01
K_{IC} [MPa·m$^{1/2}$] +22 °C	0.54 ± 0.04	0.7 ± 0.05	0.83 ± 0.03	0.86 ± 0.05
K_{IC} [MPa·m$^{1/2}$] +90 °C	0.86 ± 0.07	0.96 ± 0.04	1.11 ± 0.03	1.06 ± 0.05
G_{IC} [J/m^2] −196 °C	**154.8 ± 3.7**	348.8 ± 0.7	**558.1 ± 12.6**	444.1 ± 1.4
G_{IC} [J/m^2] −50 °C	**145.1 ± 0.3**	181.29 ± 0.2	198.9 ± 0.3	234.5 ± 0.0
G_{IC} [J/m^2] +22 °C	89.1 ± 0.5	153.34 ± 0.8	225.5 ± 0.3	250.7 ± 0.9
G_{IC} [J/m^2] +90 °C	313.4 ± 2.1	382.2 ± 0.7	533.3 ± 0.4	507.8 ± 1.2

To support the presence of the fracture phenomena, as well as the non-expected enhancement of the materials toughness in cryogenics, SEM micrographs were taken.

increased here. However, in one of our previous publications, it was shown that crack propagation rates in dynamic testing were drastically higher even at −50 °C [64]. This suggests that although K_{IC} and G_{IC} are increased at high and low temperatures, crack propagation through the material is much faster at low temperatures, emphasizing the need for suitable tougheners for low temperatures.

At 1 vol% of W36, strong shear bands appear in the material, expressing the tendency of the material to yield between finely dispersed particles in the material. As the temperature decreases from right to left, the amount and shape of the shear bands changes and disappears completely in the cryogenic test environment. This phenomenon can be explained by a change in the energy dissipation mechanism, which is highlighted and explained in Fig. 7 below. At 3 vol% W36, the shear band formation is much more pronounced than at 1 vol% and the river lines are clearly visible even at −196 °C. This amount seems to act as a threshold required for yielding to occur between particles to bridge the cracks and dissipate more energy. At 5 vol% the fracture surfaces show the same trend as at 3 vol% but it is visible that the surfaces do not increase the roughness. When the fracture surfaces are analyzed in detail, several effects can be explained. The reason why the macroscopic fracture lines disappear at −196 °C compared to the reference and the K_{IC} and G_{IC} are still higher is as follows: there is a change in the energy dissipation mechanism from shear banding to crack pinning at 1 vol% from −50 to −196 °C. Crack pinning effects are visible around the particles (highlighted with arrows) that dissipate the energy of the crack propagating through the material.

One interpretation would be a dissipating effect of energy from river lines, macroscopic shear yielding to local crack pinning around the particles (see 1 vol% at −196 °C). This crack pinning is also known from inorganic non-deformable nano-silica particles [21,65–67]. When increasing the amount of W36 to 3% by volume, the river lines reappear between the particles as previously described. This can be seen as a stronger tendency of the bulk material to allow a certain yielding under deformation, which increases the fracture toughness and energy, and

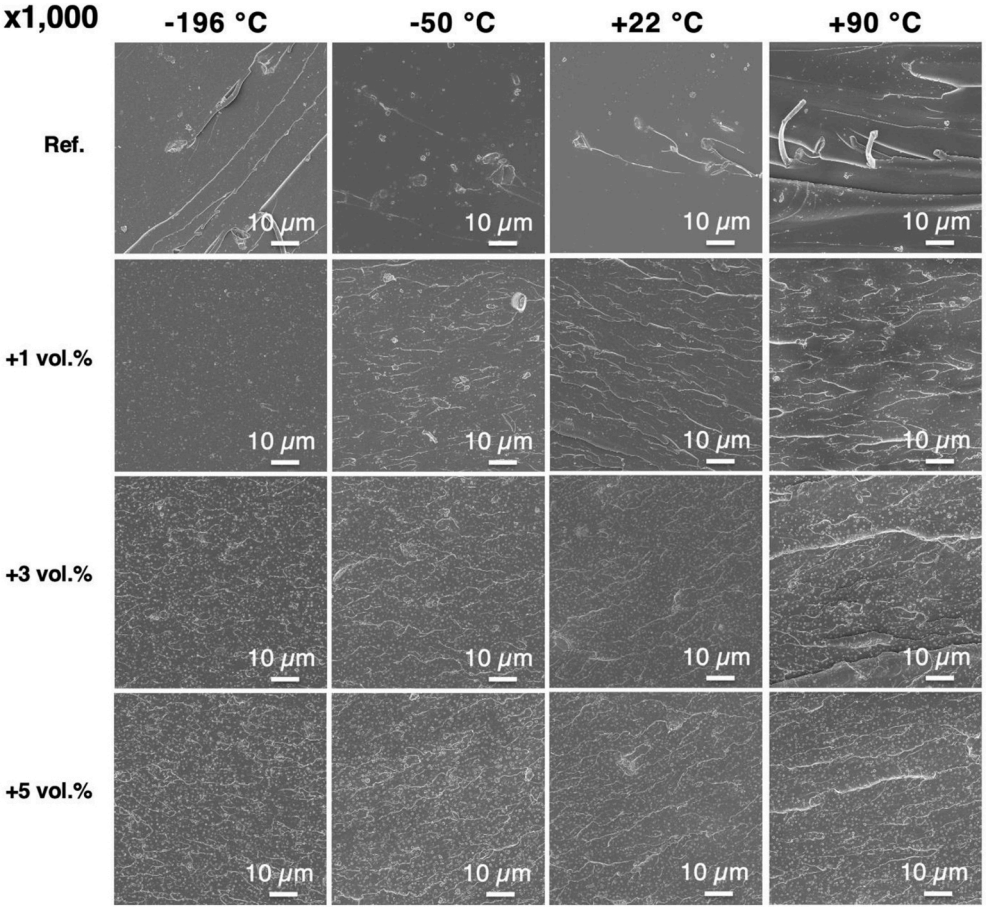

Fig. 6. Surveying fractographies of tested K_{IC} samples Reference, 1, 3 and 5 vol% at different temperatures with a magnification of x1,000 taken with an Inlens detector. The crack propagation took place from left to right.

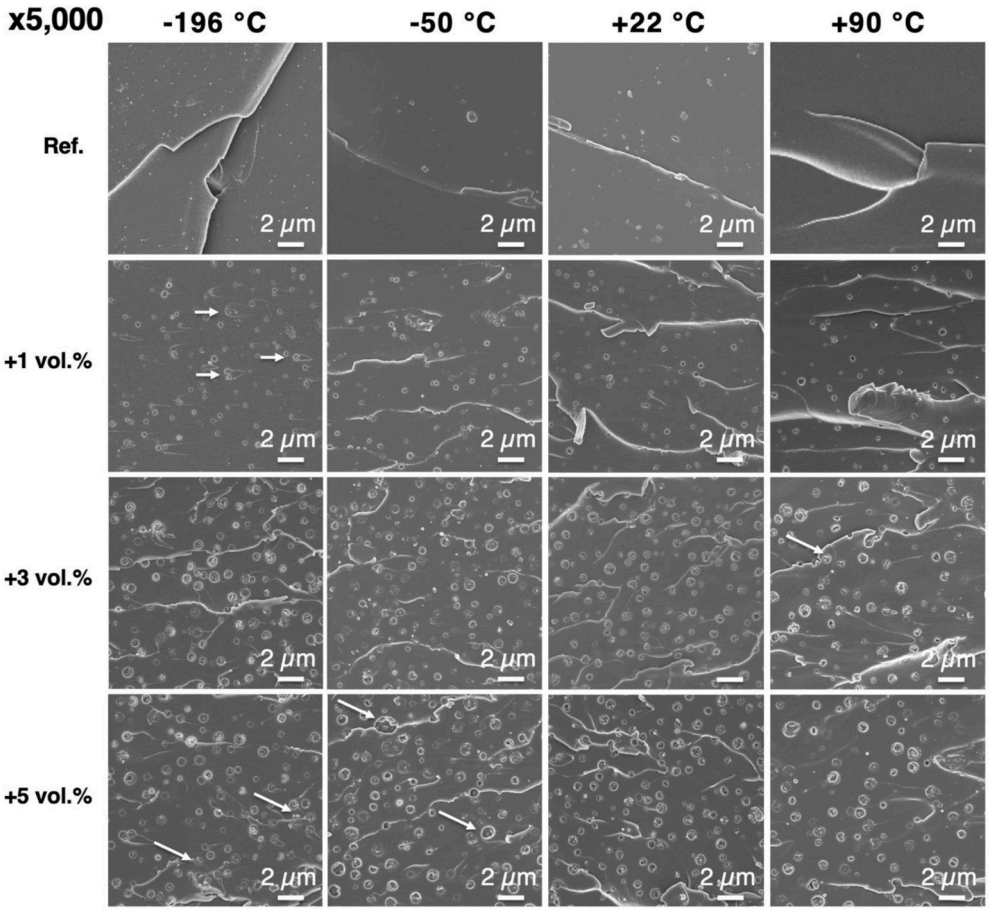

Fig. 7. Detailed fractographies of tested K_{IC} samples Reference, 1, 3 and 5 vol% at different temperatures with a magnification of x5,000 taken with an Inlens detector. The crack propagation took place from left to right.

thus potentially the resistance to microcracking under deformation in fiber composite parts. It should be noted, however, that the values tend to plateau or decrease at 5 vol% of additives.

This can also be explained with a detailed look at the highlighted fractography in Fig. 8a) and b). With increasing amount, the nano additive tends to agglomerate to form larger "grape-like" structures resulting in higher particles sizes, which means that the interparticle distance responsible for bridging the crack [68] stops decreasing. It becomes apparent, that the agglomeration of this nano additive is the reason why the K_{IC} is limited to a certain level here. Still, the positive effect of those core-shell particles on the macroscopic toughness is demonstrated at −196 °C, even though the polymeric cores (T_g around −120 °C) are frozen but show a tendency to flexibilize the epoxy resin as a bulk material. Comparing Fig. 8a) and b), also particle pull-out is a mechanism of fracture toughening, represented by the holes in the fractographys.

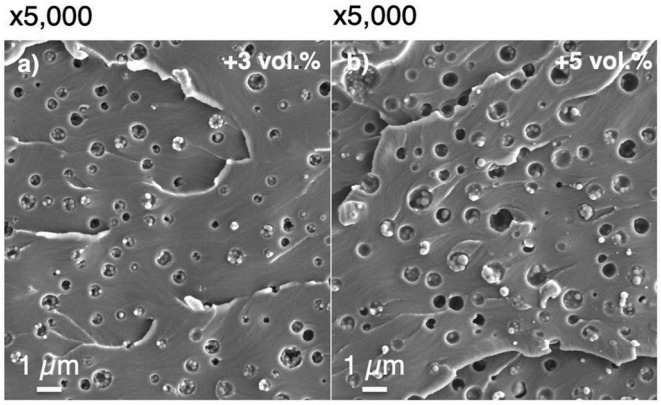

Fig. 8. a)Particle agglomeration tendency of 3 vol% W36 in EP and b) 5 vol% W36 recorded with backscattering electron detector tested at −50 °C.

4.4. Yield behavior - Compression testing & Radius of the plastic zone

The yield behavior of the materials was analyzed via stress strain curves. The total values are shown in dependency of the temperature and toughening amount in Fig. 9a) and b) below.

Here the temperature dependency follows the trend of the modulus. The compressive strength is lowest at high temperatures and increases dramatically at lower temperatures, showing a maximum at −196 °C. Remarkably, the trend is surely not linear with temperature, which is also related to the modulus, that increases strongly as soon as the aromatic structures in the structure are frozen. At −196 °C, a value of 500 MPa was reached with the reference sample, which represents an extreme increase in strength. For comparison, bulk glass is known to have a compressive strength of 1,000 MPa at room temperature, illustrating the huge increase in epoxy in LN_2. Fig. 9b) shows the impact of the toughener on the compression properties in detail. While the effect on the compressive yield strength is not strong even at −50 °C, +22 °C and +90 °C, the effect is even stronger at −196 °C. The dark blue curve shows that the compressive strength is already reduced to a minimum at 3 vol% of W36 and no longer at 5 vol%. The detailed values are shown in Table 3 and it is important to mention that the yield strength in a cryogenic environment could be reduced from 501 to 449 MPa, resulting in earlier flow of the material due to the flexibilization of the epoxy

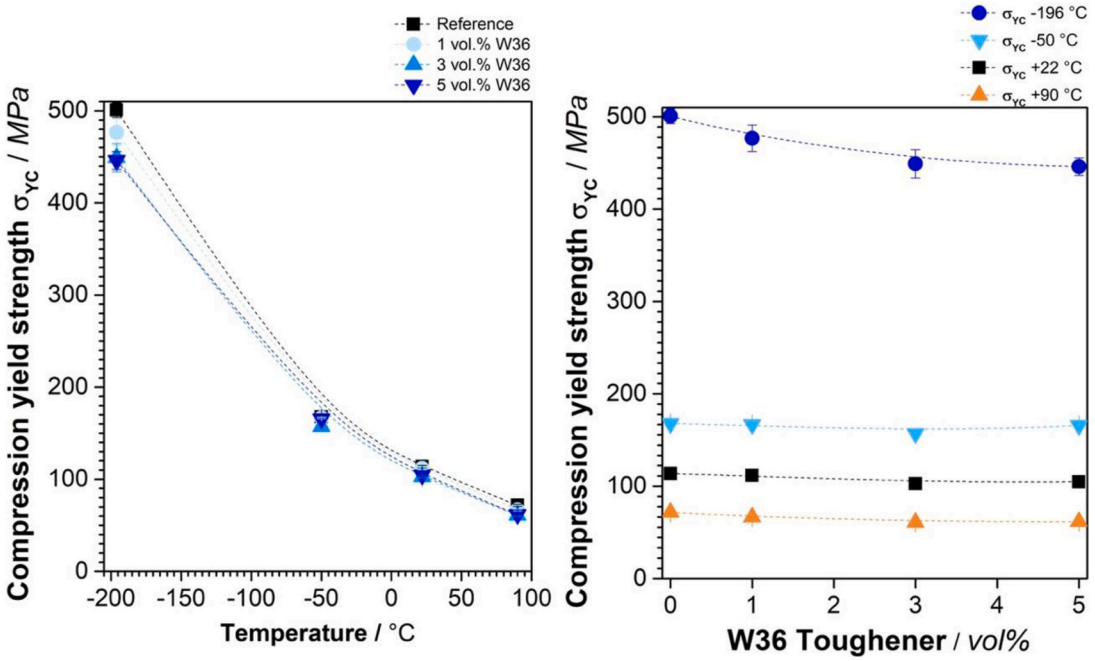

Fig. 9. a: Compression testing of the reference and toughened samples at −196 °C, −50 °C, +22 °C and +90 °C and b) highlighted influence of the toughener on the yield strength.

Table 3
Yield properties derived from compression testing.

	Reference	1 vol% W36	3 vol% W36	5 vol % W36
σ_{yc} [MPa] −196 °C	500.7 ± 7.9	467.7 ± 14.4	449.0 ± 15.3	446.7 ± 9.5
σ_{yc} [MPa] −50 °C	167.7 ± 2.4	166.7 ± 0.9	157 ± 0.1	165.7 ± 3.3
σ_{yc} [MPa] +22 °C	113.7 ± 1.2	112 ± 1.3	103 ± 1.0	104.6 ± 1.3
σ_{yc} [MPa] +90 °C	71.7 ± 1.2	66.6 ± 1.0	60.8 ± 0.6	61.6 ± 0.4
R_p [µm] −196 °C	0.4 ± 0.01	0.6 ± 0.01	**1.8 ± 0.35**	1.4 ± 0.03
R_p [µm] −50 °C	**1.9 ± 0.01**	2.3 ± 0.01	2.7 ± 0.03	2.8 ± 0.01
R_p [µm] +22 °C	1.9 ± 0.01	3.3 ± 0.01	5.5 ± 0.00	5.7 ± 0.02
R_p [µm] +90 °C	12.1 ± 0.1	17.5 ± 0.03	28.1 ± 0.02	24.1 ± 0.1

matrix caused by the siloxane particles.

Even though this tendency of an earlier yield flow behavior under load is not comparable to polymers like thermoplastics (PE, PP, e.g.), the impact on the plastic behavior is drastic for a thermoset, especially for composites. The so called plastic zone around a rack tip is responsible for a certain damage tolerance in Mode I testing of composite materials [55,69,70]. R_p was calculated and is highlighted in Fig. 10 below.

Here, the radius of the compressive strength shows a strong dependence on the plastic zone, which is also indirectly dependent on the changing modulus of the material with changing temperature. This inverse trend shows an enhanced plastic deformation behavior at +22 and + 90 °C of the resin, which is further enhanced by the incorporation of W36 particles. It can be seen, that there is no global minimum of the R_p at room temperature compared to K_{IC} or G_{IC} measurements. This can be explained by a lower modulus and reduced stiffness, which allows the material to deform plastically in theoretical calculations, meaning that the fracture energy is not linearly dependent on the plastic zone radius. By these R_p calculations, the high K_{IC} and G_{IC} values at −50 °C and especially at −196 °C must be reconsidered. The brittleness of the material, expressed in the quadrupling of the compressive strength and stiffening. This leads to a drastic drop in the quantified plasticity of the toughened resin R_p from 1.9 µm (+22 °C) to 0.4 µm (−196 °C) for the reference. However, for the best performing formulation at 3% by volume, it can be seen that R_p has increased to a level of 1.8 µm, implying that the tendency for plastic deformation in terms of crack bridging and energy dissipation is as high in this formulation in the cryogenic range as for the neat material at room temperature. A symbolized view of the cross-section of a crack passing through a composite material is shown in Fig. 11.

In a typical winded hydrogen vessel reinforced with 60 vol% intermediate modulus carbon fibers in a diameter of 5 µm, the resin-filled space in between the fibers is very small. The plastic zone in a composite is limited by the non-deformable stiff fibers. For a high interlaminar toughness, a size of 2–3 µm of the interaction zone R_p is enough to enforce yield lines and crack pinning mechanisms around and in between the particles [70]. Thus, the toughening with 3 vol% of this siloxane core-shell additive should be promising and highly performant to achieve a theoretical optimum of interlaminar crack growth resistance in cryogenic composite liquid hydrogen vessels.

5. Conclusion

A latent and sticky epoxy resin (EP) modified with siloxane core-shell particles was developed and investigated. A particular focus was on fracture toughness at cryogenic temperatures and a distinction between K_{IC}, G_{IC} and R_p. Structure-property relationships between the behavior of the molecular network and the resulting fracture properties were established. The results show that "fracture toughness" as an essential material property cannot be quantified by K_{IC} or G_{IC} alone, especially in cryogenic or high temperature environments. It is strongly dependent on the modulus and the yield strength of the resin which change drastically with temperature. Both properties, K_{IC} and σ_{yc} together determine the radius of the plastic zone R_p at the crack tip. As part of the development of a latent towpreg epoxy resin, it was possible to show that the fracture energy can also be increased at cryogenic temperatures if the flow stress of the matrix forces the resin between the particles to yield above a certain particle density. Nevertheless, fracture energy does not take the crack propagation speed into account, which strongly increases as temperature decreases. This was corroborated by CT-specimen measurements and fractographs. It was found that low T_g core of the siloxane particles have a positive plasticizing effect on the epoxy resin network, which causes a ductilized behavior even in cryogenic temperatures. The optimal value for the core-shell-particle fraction was found to be 3% by

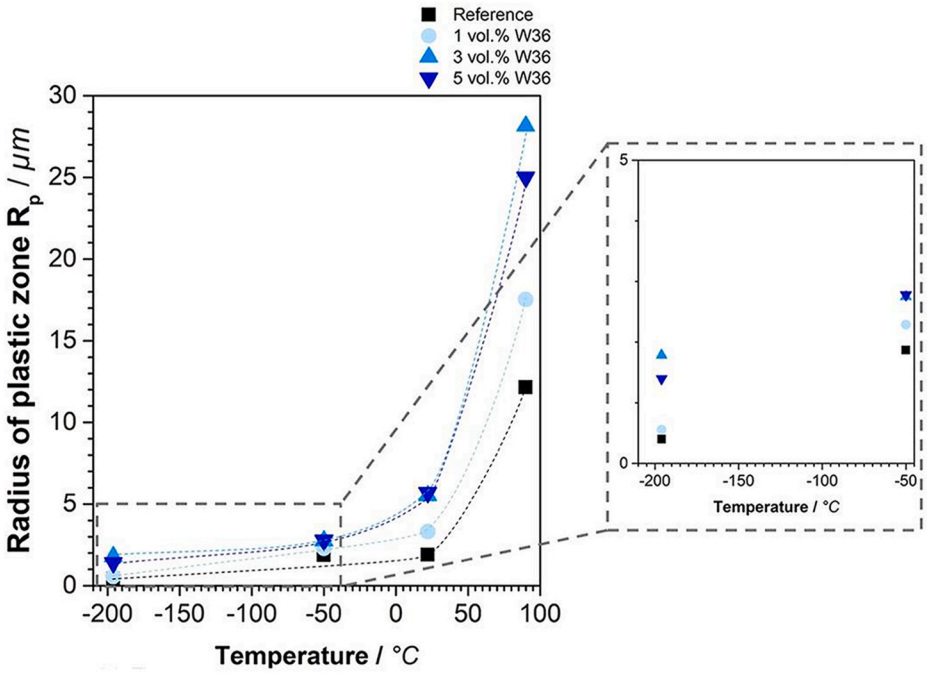

Fig. 10. Calculation of the plastic zone R_p derived from K_{IC} and yield strength at −196 °C, −50 °C, +22 °C and +90 °C.

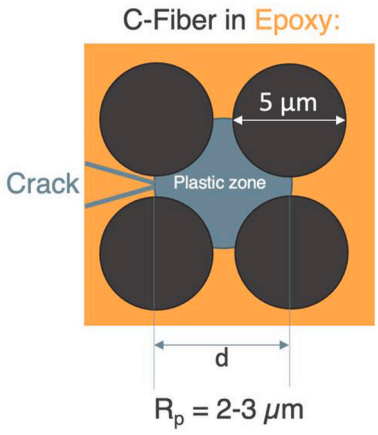

Fig. 11. Schematic of the plastic zone spreading behavior in a composite material.

volume, which led to an enormous increase of R_p from 0.4 µm to 1.8 µm in the case of cryogenic exposure.

Author statement

Fabian Hübner: Conceptualization, Investigation, Writing - Original Draft, Data Curation, Visualization, Methodology, Formal analysis. Michael Hoffmann: Investigation, Data Curation, Methodology, Nicole Sommer, Investigation, Data Curation. Andreas Scherer: Supervision, Resources. Tobias Dickhut: Supervision, Resources, Volker Altstädt, Validation, Supervision. Holger Ruckdäschel: Validation, Supervision.

Declaration of competing interest

The authors declare that they have no known competing financial interests or personal relationships that could have appeared to influence the work reported in this paper.

Acknowledgement

This study was funded within the project "*CryoFuselage*", LAB-AY108A that was financially supported by *Bavarian Federal* Ministry of Economic Affairs and Energy (StMWi) and guided by German Aerospace Center (DLR). We highly gratitude Annika Pfaffenberger for the series of SEM fractographies, Ute Kuhn for DMTA measurements, Andreas Mainz for support in mechanical testing and implementation as well as Wacker, Olin Epoxy and Alzchem for sample supply.

References

[1] Handbuch AVK, Faserverbundkunststoffe/Composites, Hanser Publishers, Munich, 2013.
[2] R.R. Boyer, J.D. Cotton, M. Mohaghegh, R.E. Schafrik, Materials considerations for aerospace applications, MRS Bull. 40 (12) (2015) 1055–1065, https://doi.org/10.1557/mrs.2015.278.
[3] G.W. Ehrenstein, Faserverbund-Kunststoffe, Carl Hanser Verlag GmbH & Co. KG, 2006.
[4] B.S. Kim, B.H. Kim, J.B. Kim, C.R. Joe, Study on the development of composite CNG pressure vessels, Cryogenics (Guildf). 38 (1) (1998) 131–134, https://doi.org/10.1016/S0011-2275(97)00123-9.
[5] D. Leh, P. Saffré, P. Francescato, R. Arrieux, S. Villalonga, A progressive failure analysis of a 700-bar type IV hydrogen composite pressure vessel, Int. J. Hydrogen Energy 40 (38) (2015) 13206–13214, https://doi.org/10.1016/j.ijhydene.2015.05.061.
[6] F.C. Shen, A filament-wound structure technology overview, Mater. Chem. Phys. 42 (2) (1995) 96–100, https://doi.org/10.1016/0254-0584(95)01554-X.
[7] M.G. Kim, J.S. Hong, S.G. Kang, C.G. Kim, Enhancement of the crack growth resistance of a carbon/epoxy composite by adding multi-walled carbon nanotubes at a cryogenic temperature, Compos. Part A Appl. Sci. Manuf. 39 (4) (2008) 647–654, https://doi.org/10.1016/j.compositesa.2007.07.017.
[8] X. Jia, et al., Effect of geometric factor, winding angle and pre-crack angle on quasi-static crushing behavior of filament wound CFRP cylinder, Compos. B Eng. 45 (1) (2013) 1336–1343, https://doi.org/10.1016/j.compositesb.2012.09.060.
[9] C. Kaynak, E.S. Erdiller, L. Parnas, F. Senel, Use of split-disk tests for the process parameters of filament wound epoxy composite tubes, Polym. Test. 24 (5) (2005) 648–655, https://doi.org/10.1016/j.polymertesting.2005.03.012.
[10] H. Otsubo, M. Mizuno, Y. Negishi, N. Ogami, High-pressure hydrogen tank for FCHV, *SAE Tech. Pap.*, no. Figure 1 (2007) 548–553, https://doi.org/10.4271/2007-01-2009.
[11] Y. Nonobe, Development of the fuel cell vehicle mirai, IEEJ Trans. Electr. Electron. Eng. 12 (1) (2017) 5–9, https://doi.org/10.1002/tee.22328.
[12] Y.X. He, et al., Micro-crack behavior of carbon fiber reinforced thermoplastic modified epoxy composites for cryogenic applications, Compos. B Eng. 44 (1) (2013) 533–539, https://doi.org/10.1016/j.compositesb.2012.03.014.

[13] S. Villalonga, et al., Composite 700 bar-vessel for on-board compressed gaseous hydrogen storage, ICCM Int. Conf. Compos. Mater. (2009).
[14] B. Zohuri, Hydrogen Energy - Challenges and Solutions for a Cleaner Future, Springer Nature Switzerland AG, Cham, Switzerland, 2019.
[15] J.F. Timmerman, B.S. Hayes, J.C. Seferis, Cryogenic microcracking of carbon fiber/epoxy composites: influences of fiber-matrix adhesion, J. Compos. Mater. 37 (21) (2003) 1939–1950, https://doi.org/10.1177/002199803036281.
[16] J.F. Timmerman, M.S. Tillman, B.S. Hayes, J.C. Seferis, Nanoclay reinforcement effects on the cryogenic microcracking of carbon fiber/epoxy composites, Polymer (Guildf). 33 (2002) 323–329.
[17] H. Kishi, S. Matsuda, J. Imade, Y. Shimoda, T. Nakagawa, Y. Furukawa, Fatigue resistance of toughened epoxy resins modified with preformed polymer particles, Seville, Spain, 22-26 June 2014, in: ECCM16 - 16TH EUROPEAN CONFERENCE ON COMPOSITE MATERIALS, 12, 2014, pp. 22–26. June.
[18] A.J. Kinloch, A.C. Taylor, M. Techapaitoon, W.S. Teo, S. Sprenger, From matrix nano- and micro-phase toughening to composite macro-properties, 2071, Philos. Trans. R. Soc. A Math. Phys. Eng. Sci. 374 (2016), https://doi.org/10.1098/rsta.2015.0275.
[19] J.K. Huang, A. Kinloch, The role of plastic void growth in the fracture of rubber-toughened epoxy polymers, J. Mater. Sci. Lett. 11 (1992) 484–487, https://doi.org/10.1007/BF00731112.
[20] R.J. Varley, Toughening of epoxy resin systems using low-viscosity additives, Polym. Int. 53 (1) (2004) 78–84, https://doi.org/10.1002/pi.1321.
[21] S. Sprenger, Improving mechanical properties of fiber-reinforced composites based on epoxy resins containing industrial surface-modified silica nanoparticles: review and outlook, J. Compos. Mater. 49 (1) (2015) 53–63, https://doi.org/10.1177/0021998313514260.
[22] A.J. Kinloch, R.D. Mohammed, A.C. Taylor, C. Eger, S. Sprenger, D. Egan, The effect of silica nano particles and rubber particles on the toughness of multiphase thermosetting epoxy polymers, J. Mater. Sci. 40 (18) (2005) 5083–5086, https://doi.org/10.1007/s10853-005-1716-2.
[23] T.H. Hsieh, A.J. Kinloch, K. Masania, A.C. Taylor, S. Sprenger, The mechanisms and mechanics of the toughening of epoxy polymers modified with silica nanoparticles, Polymer (Guildf). 52 (12) (2010) 2518–2522, https://doi.org/10.1002/pen.23211.
[24] Z.K. Chen, J.P. Yang, Q.Q. Ni, S.Y. Fu, Y.G. Huang, Reinforcement of epoxy resins with multi-walled carbon nanotubes for enhancing cryogenic mechanical properties, Polymer (Guildf) 50 (19) (2009) 4753–4759, https://doi.org/10.1016/j.polymer.2009.08.001.
[25] N. Domun, H. Hadavinia, T. Zhang, T. Sainsbury, G.H. Liaghat, S. Vahid, Improving the fracture toughness and the strength of epoxy using nanomaterials-a review of the current status, Nanoscale 7 (23) (2015) 10294–10329, https://doi.org/10.1039/c5nr01354b.
[26] F. Sawa, S. Nishijima, T. Okada, Molecular design of an epoxy for cryogenic temperatures, Cryogenics (Guildf). 35 (11) (1995) 767–769, https://doi.org/10.1016/0011-2275(95)90910-8.
[27] F. Sawa, S. Nishijima, Y. Ohtani, K. Matsushita, T. Okada, Fracture toughness and relaxation of epoxy resins at cryogenic temperatures, Adv. Cryog. Eng. Mater. 40 (1994) 1113–1119, https://doi.org/10.1007/978-1-4757-9053-5_141.
[28] B.C. Kim, S.W. Park, D.G. Lee, Fracture toughness of the nano-particle reinforced epoxy composite, Compos. Struct. 86 (1–3) (2008) 69–77, https://doi.org/10.1016/j.compstruct.2008.03.005.
[29] Y. Zhao, et al., Effect of free volume on cryogenic mechanical properties of epoxy resin reinforced by hyperbranched polymers, Mater. Des. 202 (2021), 109565, https://doi.org/10.1016/j.matdes.2021.109565.
[30] G. Yang, S.Y. Fu, J.P. Yang, Preparation and mechanical properties of modified epoxy resins with flexible diamines, Polymer (Guildf). 48 (1) (2007) 302–310, https://doi.org/10.1016/j.polymer.2006.11.031.
[31] H.R. Brown, Investigation of the Deformation Mechanisms of Core-Shell Rubber-Modified Epoxy at Cryogenic Temperatures, Mississippi State University, 2012.
[32] S. Li, H. Wang, M. Liu, C. Peng, Z. Wu, Epoxy-functionalized Polysiloxane Reinforced Epoxy Resin for Cryogenic Application, 46930, 2018, pp. 1–9, https://doi.org/10.1002/app.46930.
[33] Z. Zhou, et al., Phosphorus and bromine modified epoxy resin with enhanced cryogenic mechanical properties and liquid oxygen compatibility simultaneously, Polym. Test. 94 (2021), 107051, https://doi.org/10.1016/j.polymertesting.2021.107051.
[34] G. Hartwig, Low-temperature properties of epoxy resins and composites, Adv. Cryog. Eng. 24 (1978) 17–36, https://doi.org/10.1007/978-1-4613-9853-0_2.
[35] Y. Zhao, Z.K. Chen, Y. Liu, H.M. Xiao, Q.P. Feng, S.Y. Fu, Simultaneously enhanced cryogenic tensile strength and fracture toughness of epoxy resins by carboxylic nitrile-butadiene nano-rubber, Compos. Part A Appl. Sci. Manuf. 55 (2013) 178–187, https://doi.org/10.1016/j.compositesa.2013.09.005.
[36] T. Ueki, S. Nishijima, Y. Izumi, Designing of epoxy resin systems for cryogenic use, Cryogenics (Guildf). 45 (2) (2005) 141–148, https://doi.org/10.1016/j.cryogenics.2004.07.002.
[37] F. Hübner, J. Meuchelböck, F. Wolff-fabris, M. Mühlbach, V. Altstädt, H. Ruckdäschel, Fast curing unidirectional carbon epoxy prepregs based on a semi-latent hardener: the influence of ambient aging on the prepregs Tg0 , processing behavior and thus derived interlaminar performance of the composite, Compos. Sci. Technol. 216 (2021), https://doi.org/10.1016/j.compscitech.2021.109047.
[38] Alzchem Trostberg GmbH, "DYHARD Product Line Resin Additives AlzChem." .
[39] L.V. Chursova, A.I. Tkachuk, N.N. Panina, Y.M. Gurevich, A.N. Babin, G.V. Malkov, A study of the mechanism of curing of the dicyandiamide-epoxydiane oligomer system in the presence of asymmetrical urea, Polym. Sci. Ser. D 8 (2) (2015) 153–162, https://doi.org/10.1134/s1995421215020057.
[40] T. Güthner, B. Hammer, Curing of epoxy resins with dicyandiamide and urons, J. Appl. Polym. Sci. 50 (4) (1993) 1453–1459.
[41] M. Hayaty, H. Honarkar, M.H. Beheshty, Curing behavior of dicyandiamide/epoxy resin system using different accelerators," *Iran*, Polym. J. (English Ed. 22 (8) (2013) 591–598, https://doi.org/10.1007/s13726-013-0158-y.
[42] N. Poisson, A. Maazouz, H. Sautereau, M. Taha, X. Gambert, Curing of dicyandiamide epoxy resins accelerated with substituted ureas, J. Appl. Polym. Sci. 69 (12) (1998) 2487–2497.
[43] T.F. Saunders, M.F. Levy, J.F. Serino, Mechanism of the tertiary amine-catalyzed dicyandiamide cure of epoxy resins, J. Polym. Sci. 1 Polym. Chem. 5 (7) (1967) 1609–1617, https://doi.org/10.1002/pol.1967.150050711.
[44] Wacker Chemie AG, "Technical Datasheet Genioperl ® W36," Munich, 2019.
[45] F. Hübner, E. Szpoganicz, M. Demleitner, J. Kuhnigk, V. Altstädt, A. Rios de Anda, Time domain 1 H NMR, thermomechanical, and rheology multiscale structural characterization of polydimethylsiloxane-toughened epoxy nanocomposites for liquid composite molding, ACS Appl. Polym. Mater. (2020), https://doi.org/10.1021/acsapm.0c00763.
[46] H.R. Brown, J.A. Schneider, T.L. Murphy, Experimental studies of the deformation mechanisms of core-shell rubber-modified diglycidyl ether of bisphenol-A epoxy at cryogenic temperatures, J. Compos. Mater. 48 (11) (2014) 1279–1296, https://doi.org/10.1177/0021998313485262.
[47] J. Wang, D. Magee, J.A. Schneider, Dynamic mechanical properties and fracture surface morphologies of core-shell rubber (CSR) toughened epoxy at Liquid Nitrogen (LN2) temperatures, Int. SAMPE Symp. Exhib. 54 (2009) 12–13.
[48] J. Chen, Toughening epoxy polymers and carbon fibre composites with core-shell particles, block copolymers and silica nanoparticles, no. July, Mech. Eng. Dep. Imp. Coll. London, PhD (2013).
[49] W. Grellmann, S. Seidler, Kunststoffprüfung, third ed., Hanser, Munich, 2015.
[50] M.H. Kothmann, R. Zeiler, A. Rios De Anda, A. Brückner, V. Altstädt, Fatigue crack propagation behaviour of epoxy resins modified with silica-nanoparticles, Polymer (Guildf). 60 (2015) 157–163, https://doi.org/10.1016/j.polymer.2015.01.036.
[51] K. Saalwächter, Proton multiple-quantum NMR for the study of chain dynamics and structural constraints in polymeric soft materials, Prog. Nucl. Magn. Reson. Spectrosc. 51 (1) (2007) 1–35, https://doi.org/10.1016/j.pnmrs.2007.01.001.
[52] L. Monnerie, F. Lauprêtre, J.L. Halary, Investigation of solid-state transitions in linear and crosslinked amorphous polymers, October, Adv. Polym. Sci. 187 (2005) 35–213, https://doi.org/10.1007/b136955.
[53] M.K. Hassan, S.J. Tucker, A. Abukmail, J.S. Wiggins, K.A. Mauritz, Polymer chain dynamics in epoxy based composites as investigated by broadband dielectric spectroscopy, Arab. J. Chem. 9 (2) (2016) 305–315, https://doi.org/10.1016/j.arabjc.2015.07.016.
[54] T. Saatkamp, Bruchverhalten von Polymeren bei kryogenen Temperaturen Kernforschungszentrum Karlsruhe, University of Karlsruhe, 1991.
[55] A.C.T.T.H. Hsieh, A.J. Kinloch*, K. Masania, The mechanisms and mechanics of the toughening of epoxy polymers modified with silica nanoparticles, Polym. Eng. Sci. 52 (12) (2012) 2518–2522, https://doi.org/10.1002/pen.23211.
[56] A. Arbor, Rate and temperature effects on the fracture toughness of a rubber - modified epoxy, Polymer (Guildf). 34 (8) (1993) 1695–1701, https://doi.org/10.1016/0032-3861(93)90329-9.
[57] G. Giannakopoulos, K. Masania, A.C. Taylor, Toughening of epoxy using core-shell particles, J. Mater. Sci. 46 (2) (2011) 327–338, https://doi.org/10.1007/s10853-010-4816-6.
[58] J.N. Sultan, F.J. McGarry, Effect of rubber particle size on deformation mechanisms in glassy epoxy, Polym. Eng. Sci. 13 (1) (1973) 29–34, https://doi.org/10.1002/pen.760130105.
[59] A. Bajpai, B. Wetzel, K. Friedrich, High strength epoxy system modified with soft block copolymer and stiff core-shell rubber nanoparticles: morphology, mechanical properties, and fracture mechanisms, Express Polym. Lett. 14 (4) (2020) 384–399, https://doi.org/10.3144/expresspolymlett.2020.32.
[60] G.W. Ehrenstein, G. Riedel, P. Trawiel, Thermal Analysis of Plastics - Theory and Practice, Hanser, Munich, Germany, 2004.
[61] H. Nakane, S. Nishijima, H. Fujishiro, T. Yamaguchi, S. Yoshizawa, S. Yamazaki, Thermal Properties of Epoxy Resins at Cryogenic Temperatures, 211, 2002, https://doi.org/10.1063/1.1472545.
[62] G. Christoph, Bruchprozesse von Polymeren bei tiefen Temperaturen, 1996.
[63] J.W. Yi, Y.J. Lee, W. Lee, S.B. Lee, M.K. Um, Cryogenic Thermal Expansion and Mechanical Properties of Epoxy Resin Modified with Polydimethylsiloxane, June, 2012, pp. 24–28.
[64] F. Hübner, A. Brückner, T. Dickhut, V. Altstädt, A.R. de Anda, H. Ruckdäschel, Low temperature fatigue crack propagation in toughened epoxy resins aimed for filament winding of type V composite pressure vessels, October, Polym. Test. 102 (2021), https://doi.org/10.1016/j.polymertesting.2021.107323.

[65] M.H. Kothmann, M. Ziadeh, G. Bakis, A. Rios de Anda, J. Breu, V. Altstädt, Analyzing the influence of particle size and stiffness state of the nanofiller on the mechanical properties of epoxy/clay nanocomposites using a novel shear-stiff nano-mica, J. Mater. Sci. 50 (14) (2015) 4845–4859, https://doi.org/10.1007/s10853-015-9028-7.

[66] S. Li, Q. Wu, H. Zhu, Q. Lin, C. Wang, Impact resistance enhancement by adding core-shell particle to epoxy resin modified with hyperbranched polymer, 12, Polymers (Basel) 9 (2017), https://doi.org/10.3390/polym9120684.

[67] S. Sprenger, Epoxy resin composites with surface-modified silicon dioxide nanoparticles: a review, J. Appl. Polym. Sci. 130 (3) (2013) 1421–1428, https://doi.org/10.1002/app.39208.

[68] R. Bagheri, R.A. Pearson, Role of particle cavitation in rubber-toughened epoxies : II. Inter-particle distance, Polymer (Guildf). 41 (2000) 269–276, https://doi.org/10.1016/S0032-3861(99)00126-3.

[69] V. Altstädt, Effect of the polymer matrix on the properties of advanced composites, Makromol. Chemie. Macromol. Symp. 50 (1) (1991) 137–145, https://doi.org/10.1002/masy.19910500114.

[70] V. Altstädt, D. Gerth, M. Stängle, H.G. Recker, Interlaminar crack growth in third-generation thermoset prepreg systems, Polymer (Guildf). 34 (4) (1993) 907–909, https://doi.org/10.1016/0032-3861(93)90379-O.